Irinophore C, a Novel Nanoformulation of Irinotecan, Alters Tumor Vascular Function and Enhances the Distribution of 5-Fluorouracil and Doxorubicin

Jennifer H.E. Baker,[1] Jeffrey Lam,[2] Alaistair H. Kyle,[1] Jonathan Sy,[1] Thomas Oliver,[2] Steven J. Co,[2] Wieslawa H. Dragowska,[2] Euan Ramsay,[2] Malathi Anantha,[2] Thomas J. Ruth,[3] Michael J. Adam,[3] Andrew Yung,[4] Piotr Kozlowski,[4] Andrew I. Minchinton,[1,5] Sylvia S.W. Ng,[2,6] Marcel B. Bally,[2,5,6] and Donald T.T. Yapp[2,6]

Abstract

Purpose: To examine the antitumor effects of Irinophore C, a nanopharmaceutical formulation of irinotecan, on the tissue morphology and function of tumor vasculature in HT-29 human colorectal tumors.

Experimental Design: Fluorescence microscopy was used to map and quantify changes in tissue density, tumor vasculature, hypoxia, and the distribution of Hoechst 33342, a perfusion marker, and the anticancer drug, doxorubicin. Noninvasive magnetic resonance imaging was used to quantify K_{trans}, the volume transfer constant of a solute between the blood vessels and extracellular tissue compartment of the tumor, as a measure of vascular function. Following treatment with Irinophore C, ^{19}F magnetic resonance spectroscopy was used to monitor the delivery of 5-fluorouracil (5-FU) to the tumor tissue, whereas scintigraphy was used to quantify the presence of bound [^{14}C]5-FU.

Results: Irinophore C decreased cell density ($P = 8.42 \times 10^{-5}$), the overall number of endothelial cells in the entire section ($P = 0.014$), tumor hypoxia ($P = 5.32 \times 10^{-9}$), and K_{trans} ($P = 0.050$). However, treatment increased the ratio of endothelial cells to cell density ($P = 0.00024$) and the accumulation of Hoechst 33342 ($P = 0.022$), doxorubicin ($P = 0.243 \times 10^{-5}$), and 5-FU ($P = 0.0002$) in the tumor. Vascular endothelial growth factor and interleukin-8, two proangiogenic factors, were down-regulated, whereas the antiangiogenic factor TIMP-1 was up-regulated in Irinophore C-treated tumors.

Conclusions: Irinophore C treatment improves the vascular function of the tumor, thereby reducing tumor hypoxia and increasing the delivery and accumulation of a second drug. Reducing hypoxia would enhance radiotherapy, whereas improving delivery of a second drug to the tumor should result in higher cell kill.

The clinical management of metastatic disease originating from colon/colorectal cancer remains challenging. The liver is the most common site of distant metastases for colorectal cancer, with 70% of patients presenting with liver metastases followed by the lungs, bone, and brain (1, 2). At present, the only cure is complete surgical removal of the primary tumor if diagnosed early; however, up to 45% of these patients still relapse with metastatic disease. Standard of care for first-line therapy in patients is a combination of 5-fluorouracil (5-FU; plus leucovorin) with either irinotecan (FOLFIRI) or oxaliplatin (FOLFOX; ref. 3). The treatments are associated with prolonged median survivals of 18 to 21 months. Capecitabine, an oral fluoropyrimidine carbamate, has also been used in combination with 5-FU, and clinical data suggest that this combination is comparable with the FOLFIRI and FOLFOX regimens (4, 5). In practice, however, combination therapy with capecitabine is limited because of severe toxicities such as hand-foot syndrome, diarrhea, nausea, vomiting, and bone marrow suppression (4, 5). More recently, monoclonal antibodies targeting the epidermal growth factor receptor, such as cetuximab and panitumumab, have been used in combination with standard chemotherapy with promising results (6). The safety and efficacy of bevacizumab, the monoclonal antibody that targets vascular endothelial growth factor (VEGF; ref. 7), in combination with FOLFIRI or FOLFOX, was also evaluated recently (8, 9). Although both studies were carried out with small

Authors' Affiliations: [1]Medical Biophysics, [2]Advanced Therapeutics (BC Cancer Agency), [3]Department of Life Sciences (TRIUMF), [4]High Field MRI Centre, [5]Faculty of Pathology and Laboratory Sciences, and [6]Division of Pharmaceutics and Biopharmaceutics, Faculty of Pharmaceutical Sciences, University of British Columbia, Vancouver, British Columbia, Canada

Received 3/20/08; revised 8/12/08; accepted 8/13/08.

Grant support: Canadian Institutes of Health Research (M.B. Bally and A.I. Minchinton); Cancer Research Society and Rethink Breast Cancer (D.T.T. Yapp); and Michael Smith Foundation for Health Research (J.H.E. Baker and A.H. Kyle).

The costs of publication of this article were defrayed in part by the payment of page charges. This article must therefore be hereby marked *advertisement* in accordance with 18 U.S.C. Section 1734 solely to indicate this fact.

Requests for reprints: Donald T.T. Yapp, Advanced Therapeutics (BC Cancer Agency), 675 West 10th Avenue, Vancouver, British Columbia V5Z 1L3, Canada. Phone: 604-675-8023; Fax: 604-675-8183; E-mail: dyapp@bccrc.ca.

doi:10.1158/1078-0432.CCR-08-0736

Translational Relevance

Median survival times of 18 to 21 months are associated with irinotecan-based treatments for metastatic colorectal cancer. We report here a novel formulation of irinotecan, Irinophore C, which improves oxygenation levels and the delivery and accumulation of a second drug in a tumor model for colorectal cancer. Increasing oxygen levels would potentiate radiotherapy, and improving delivery of a second drug should increase cell kill. If human tumors respond similarly to Irinophore C, replacing irinotecan with Irinophore C in current combination therapies could improve the delivery of the partner agents (oxaliplatin, 5-FU, or leucovorin). Imaging techniques (magnetic resonance imaging and positron emission tomography) could be used to monitor changes in the tumor and help delineate the use of sequential therapies to target specific treatment induced changes in the tumor microenvironment (e.g., radiotherapy when oxygen levels improve). Integrating Irinophore C into clinical use should be relatively easy because irinotecan is clinically approved for colorectal cancer.

patient numbers, Kang et al. concluded that the combination treatment had modest activity and was relatively tolerable in metastatic colorectal cancer that had failed FOLFIRI or FOLFOX. A retrospective study where bevacizumab and FOLFOX were used in first-line treatment of metastatic colorectal cancer (8) further indicated that the treatment improved time to disease progression and overall survival. The authors concluded that this combination should be explored further. Finally, there is interest in using radiotherapy concurrently with chemotherapy in an adjuvant setting (10, 11).

Of particular interest to our group, the positive results with the antiangiogenic activity of bevacizumab indicate that the vasculature of colorectal tumors is an important therapeutic target in metastatic colorectal cancer. The clinical utility of combination therapies underlines the fact that novel approaches targeting more than one of the hallmarks of aggressive cancer should be explored more fully. More specifically, there is interest in targeting tumor vasculature and cancer cells in combination. Thus, for example, vascular disrupting agents have been used as single agents to shut down blood vessels in tumors and also in combination with chemotherapy (12, 13). The utility of antiangiogenic agents in clinical trials as single agents and in combination with chemoradiation is also being examined (14, 15).

Although newer treatments have improved the outcome of metastatic colorectal cancer from 6 months without treatment to 2 years with treatment, we believe that further improvements in survival time are achievable using innovative therapeutics and carefully designed treatment scheduling. An attractive proposition is to devise a sequence of therapies designed to take advantage of treatment-induced changes in the tumor microenvironment that can be readily measured using noninvasive imaging methods. We recently reported on the improved efficacy of a novel lipid-based formulation of irinotecan (Irinophore C) where treatment outcomes in 5 xenograft models, including the HT-29 and LS-180 models for colorectal cancer, were significantly improved (16, 17). In brief, the difference in pharmacokinetic profiles between free Irinotecan (Camptosar) and Irinophore C is best emphasized by the 1,000-fold increase in the plasma area-under-the-curve of the lactone form of irinotecan, the active form of the drug, seen with Irinophore C compared with that of Camptosar. Irinotecan is also metabolized by carboxylesterase to yield SN-38, which is 100- to 1,000-fold more potent *in vitro* than the parent drug. Like irinotecan, SN-38 also exists in equilibrium as the lactone and carboxylate forms, and we have also shown that both forms of SN-38 were detected in the plasma 5 min after injection of Camptosar. In contrast, only the lactone form was detected in the plasma following Irinophore C administration. The plasma levels of SN-38 lactone peaked at 2 μg/mL within 1 h, decreased to 1 μg/mL after 4 h, and remained constant thereafter over 24 h; however, the plasma concentrations of SN-38 at 24 h were still greater than those observed for Camptosar 10 min after administration.

To gain a better understanding of the mechanism behind the antitumor activity of Irinophore C, we examined the treatment-induced effects on the tumor microenvironment in the HT-29 colorectal cancer model. Our interest in assessing the tumor microenvironment was driven in part by publications suggesting that irinotecan inhibits angiogenesis (18) and also by the potential for systemically administered nanopharmaceuticals to achieve antivascular effects comparable with those achieved with metronomic dosing (19). The studies described here used multimodality imaging methods to assess tumor-associated vascular structure and function. These include noninvasive magnetic resonance imaging/spectroscopy and tumor mapping of biological markers in tumor sections. Fluorescence microscopy and tumor mapping techniques were used to quantify the observed decreases in tumor blood vessel content, hypoxia, and viable cell density. Treatment with Irinophore C increased the accumulation of a perfusion marker (Hoechst 33342). Magnetic resonance imaging indicated that vascular function improved following treatment with Irinophore C. The vascular changes were further associated with enhanced delivery of doxorubicin and 5-FU determined with fluorescence microscopy and ^{19}F magnetic resonance spectroscopy (MRS), respectively.

Materials and Methods

Tumor model. Animal studies were approved by the University of British Columbia Animal Care Committee and conducted in accordance with guidelines from the Canadian Council for Animal Care. The HT-29 tumor model for colon cancer was used in these studies; 5×10^6 cells (50 μL medium) were injected subcutaneously into the lower backs of female Rag2M mice. Tumors appeared within 2 weeks following cell inoculation and mice were randomly separated into 7 groups at this time (6 mice per group, unless indicated otherwise). Treatments were initiated when tumors reached an average volume of ~150 mm^3 (~0.5 cm in diameter). Tumor volume was calculated as volume = 0.5 length (cm) × width $(cm)^2$. Dimensions were measured using calipers by the same technician throughout the duration of the studies.

Treatment groups and drug/marker administration. Procedures for encapsulating irinotecan in liposomes have been described previously (16). In brief, irinotecan was encapsulated in 1,2-distearoyl-*sn*-glycerophosphocholine and cholesterol distearoyl phosphatidylcholine/cholestrol at a molar ratio of 55:45. The distearoyl phosphatidylcholine/

cholestrol/cholesterol lipid films formed were hydrated at 65°C in a solution of 300 mmol/L copper sulfate solution and subjected to 5 cycles of freeze-and-thaw. The multilamellar vesicle suspensions were extruded 10 times through polycarbonate filters with defined pore size to obtain unilamellar vesicles with a mean size distribution of 100 to 140 nm. The external buffer of the liposomes was then exchanged using Sephadex G-50 size exclusion chromatography, with HEPES-buffered solution containing EDTA (pH 7.5). The liposomes were then preincubated in the presence of the divalent metal ionophore A23187 at 60°C for 30 min. Subsequently, irinotecan hydrochloride trihydrate was added to liposomes at 50°C in a drug-to-lipid ratio of 0.2:1 (mol/mol); under these conditions, >98% of the added drug associates with the liposomes. These drug-loaded liposomes are then exchanged into a non-EDTA-containing buffer and adjusted to an irinotecan concentration suitable for administration to mice. It should be noted that a scaled version of this formulation process has been developed for batch sizes of 1 L; stability studies to date suggest that the drug-loaded preparation is stable for >6 months at 4°C. The formulation was administered (25 mg/kg, active drug ingredient) to one group once a week for 3 weeks and the tumors allowed to regrow after treatment was stopped. The remaining 6 groups of mice received either saline or Irinophore C once a week for 6 weeks with a 10-day break after week 3 of the treatment regimen. The tumors in one group (and saline control group) were used to assess tumor growth delay, K_{trans} values, and levels of hypoxia. The hypoxia marker EF5 (30 mg/kg; ref. 20) and the fluorescent dye Hoechst 33342 (16 mg/kg; Sigma) were injected intravenously into mice 180 and 20 min before sacrifice, respectively. Tumors were harvested and portions were cryopreserved in tissue preservative (OCT) or flash-frozen in liquid nitrogen for subsequent molecular analysis. The remaining two groups (and controls) were used to assess the tumor accumulation of 5-FU and doxorubicin (Sigma-Aldrich). A single bolus injection of 5-FU [200 mg/kg, labeled with [^{14}C]5-FU (0.6 μCi/mL)] was administered intravenously via a catheter placed into the animal's lateral tail vein for ^{19}F MRS scans. One hour after scans were completed, the mice were euthanized and the tumors were harvested for scintillation counting. Doxorubicin (30 mg/kg) was injected intravenously 40 min before harvesting tumors that were cryopreserved (OCT) in liquid N_2 vapor. A portion of tumors from the group used to examine the distribution of 5-FU with MRS was also fixed in formalin and embedded in paraffin blocks.

Immunohistochemistry. Tumor cryosections (10 or 20 μm, as indicated) were cut using a Cryostar HM560 (Microm International), air-dried, and imaged for exogenous marker native fluorescence (Hoechst 33342 and doxorubicin, visualized at 365 and 546 nm, respectively). Sections were fixed in 50% (v/v) acetone/methanol for 10 min at room temperature and endothelial cells were stained using an antibody to PECAM/CD31 (BD Pharmingen) and fluorescent Alexa 647 secondary antibody (Invitrogen). Reduced EF5 adducts in viable hypoxic cells were stained using the monoclonal antibody specific for EF5 adducts, ELK3-51 (21), followed by a fluorescent Alexa 488 secondary. Evaluation of cell density was carried out by imaging sections following their immersion in Hoechst 33342 (8 μg/mL at 37°C) for 30 min.

Analysis of hypoxia using flow cytometry. The methods used for analyzing the hypoxic fraction of cells present in solid tumors were reported previously (22, 23). Harvested tumors were rinsed in HBSS (Stem Cell Technologies) containing 0.4% bovine serum albumin. A portion of the tumor (~25-30%) was chopped with scalpels in ice-cold HBSS-0.4% bovine serum albumin and transferred to 14 mL tubes with disaggregation mixture [HBSS-1% bovine serum albumin fraction V (Calbiochem) collagenase type 2 and 4, final concentration 250 units/mL (Worthington Biochemical)] and rotated at 37°C for 2 h. The resulting suspensions were placed in 50 μm Medicones and run (3×, 1 min each) through a Medimachine (BD Biosciences) with extensive PBS-0.1% bovine serum albumin (PBSB) washes after each run. Collected cells were washed once with PBSB. Pellets were resuspended in 2.5 mmol/L EDTA and incubated at 37°C for 5 min to reduce cell clumping. Lastly, cells were washed, resuspended in PBSB, and stored on ice for subsequent processing. Tumor cell suspensions were diluted in 0.1% trypan blue in PBS and cells were counted using a hemocytometer. Fragments of cells, erythrocytes, and cells with 2× erythrocyte volume or smaller were excluded. All flow cytometric analyses were done using the FACSCalibur (Becton Dickinson). Hypoxia was measured by detecting EF5 adducts using the ELK3-51-Cy5 antibody developed and generously provided by Dr. C.J. Koch et al. (University of Pennsylvania). Tumor cells were fixed with 2% FA, permeabilized with 1% Tween 20, and blocked overnight to reduce nonspecific binding. ELK3-51-Cy5 antibody was titrated, and the concentration with the best signal-to-noise ratio was chosen for staining. Fixed cells (5×10^6) in 300 μL were incubated with ELK3-51-Cy5 antibody (room temperature for 3 h on a rotator) and washed three times with PBSB-0.5% Tween 20, with the third wash rotating for 1 h. Finally, cells were washed and resuspended in PBSB with 1 μg/mL Sytox Green (DNA dye; Molecular Probes) and analyzed the same day on a flow cytometer. Controls for this assay consisted of cells cultured *in vitro* for 3 h with or without 200 μmol/L EF5 in normoxic (air) or hypoxic (0.005% O_2 + 99.995% N_2) conditions. Mouse cells were differentiated from tumor cells based on DNA content compared.

Image acquisition and analysis. The imaging system consists of a robotic fluorescence microscope (Zeiss Imager Z1), a cooled, monochrome CCD camera (Retiga 4000R, QImaging), a motorized slide loader and x-y stage (Ludl Electronic Products), and customized NIH-ImageJ software.[7] The system allows adjacent microscope fields of view to be photographed and automatically tiled to produce a montage of the entire tumor cryosections at a resolution of 0.75 μm/pixel for qualitative and quantitative analysis. All variables stained on the same section were imaged separately using the monochrome camera and subsequently overlaid and aligned to generate false-color images using Adobe Photoshop (CS) or for quantitative analysis examining the spatial relationships between two and three factors of interest. NIH software applications and user-supplied algorithms were used to quantify the degree of staining on images by measuring the percentage of pixels above a threshold, determined to be a minimum of SDs above background, for the markers CD31 (>7 SDs above background) and EF5 (>7 SDs above background), and intravenously administered perfusion marker Hoechst 33342 (>18 SDs above background). Accumulation of doxorubicin was quantified by determining the average intensity of doxorubicin native fluorescence for pixels located within the tumor margins, and the data were normalized to the average intensity of flooded Hoechst 33342 staining as a control for cell density. Background autofluorescence was determined similarly using tumors untreated with doxorubicin, and this average value was subtracted from doxorubicin-treated tumors. A Leica DLM-100 microscope with a RGB filter was used to image formalin-fixed, H&E-stained sections.

Magnetic resonance imaging and spectroscopy. All magnetic resonance experiments were carried out using a 7.0 Tesla MR scanner (Bruker). Signal transmission and reception was achieved with a three-turn solenoidal radiofrequency coil (1.7 cm inner diameter) with the tumor situated in its interior. This coil was tuned to the hydrogen proton frequency (300.3 MHz) for the K_{trans} measurements and to the ^{19}F frequency (282.58 MHz) for the 5-FU measurements. The K_{trans} values were obtained from serial images acquired to monitor changes in the concentration of a MR-visible contrast agent (Gd-DTPA) within each pixel during the initial uptake and subsequent washout of the agent in the tumor. The magnetic resonance imaging scans follow the protocol reported by Lyng et al. (24); briefly, mice were anesthetized with isofluorane (5% induction, 2% maintenance), a catheter was inserted into the lateral tail vein, and the tumor was placed in the solenoid coil. A proton-density weighted scan was first acquired to

[7] Public domain program developed at the NIH (http://rsb.info.nih.gov/nih-image) running on a G5 Macintosh computer (Apple).

serve as a baseline for conversion of pixel intensity to absolute concentration values of the contrast agent. A volume equivalent to 10 μL/g body weight of the contrast agent (0.3 mmol/kg Gd-DTPA in saline) was injected via the tail vein catheter for 15 to 25 s. Starting at the time of injection, a series of 41 consecutive T_1-weighted scans was acquired with each scan lasting 64 s (spin echo MSME, TR/TE = 11.9/500 ms, field of view = 4 cm, matrix = 128 × 128, slice thickness = 1.5 mm, number of slices = 12). The concentration-time curve for each pixel was fit to a two-compartment Kety model (25), which describes the pharmacokinetics of the contrast agent using two variables: v_e (volume of extracellular extravascular space) and K_{trans} (volume transfer constant between the vasculature and tissue compartment). To assess the relative amounts of 5-FU present within treated and untreated tumors in a second group of mice, 0.05 mL of 0.12 mol/L trifluoroacetic acid in a small glass sphere, placed at the bottom of the solenoid, was used as a fluorine reference. Animals were immobilized with ketamine and acepromazine (175 and 6 mg/kg, respectively). 5-FU (200 mg/kg) was injected intravenously 1 min before the start of spectroscopy measurements. Nonlocalized fluorine spectra were acquired with a bandwidth of 50 kHz, 8192 digitizer points, repetition time of 1 s, and 300 averages, leading to a time resolution of 5 min. The evolving 5-FU peak was observed at 94.1 ppm down-frequency from the trifluoroacetic acid peak. The ratio of integrals between the 5-FU peak and the trifluoroacetic acid peak was calculated to estimate the relative amount of 5-FU present in the tumor at a particular time. Scans were repeated up to a maximum of 2 h. One hour after ^{19}F MRS scans, animals were sacrificed and the tumors were harvested. The tissue was weighed and digested in 500 μL Solvable at 50°C overnight (Sigma) before the addition of EDTA (200 mmol/L, 50 μL), H_2O_2 (30%, 200 μL), and HCl (10 N, 25 μL). The digested tissue was then added to 5 mL scintillation fluid and placed in a scintillation counter (Packard Tri-carb LS 1900 TR) to evaluate the presence of bound [^{14}C]5-FU present per gram tumor tissue.

Expression levels of VEGF-A, VEGF-C, TIMP-1, and interleukin-8. Tumors were homogenized in lysis buffer (150 mmol/L NaCl, 1% NP-40, 0.5% sodium deoxycholate, 2.5 mmol/L EDTA, 0.1% SDS, Mini protease inhibitor cocktail tablets from Roche Diagnostics) using a Polytron homogenizer (Kinematica) and stored at -80°C. Protein determination was done in triplicate using a Micro BCA protein assay (Pierce). Portions of the tumor lysates were pooled and used with the TransSignal Angiogenesis Antibody Array (Panomics) to assay relative changes in proangiogenic and antiangiogenic factors according to the manufacturer's instructions. For Western blots, ~60 μg total protein was loaded and weight separated on a NuPAGE 4% to 15% Bis-Tris gel (Invitrogen). Protein was transferred to 0.45 μm nitrocellulose membranes (Invitrogen) and blocked with 5% skim milk powder in TBST [150 mmol/L NaCl, 50 mmol/L Tris, 0.1% Tween 20 (pH 7.5)] for 2 h. The membranes were then probed for VEGF-A (Santa Cruz Biotechnology), VEGF-C (Zymed), and TIMP-1 (Chemicon) expression using rabbit IgG antibodies diluted in TBST with 5% bovine serum albumin (Sigma-Aldrich) at concentrations of 1:5,000, 1:5,000, and 1:1,000, respectively. Membranes were incubated with primary antibodies overnight at 4°C with gentle shaking. Following incubation, the membrane was washed in TBST (3 × 10 min). The corresponding anti-rabbit horseradish peroxidase-conjugated secondary antibody (Promega) was applied at a 1:5,000 dilution in TBST and 3% skim milk for 1 h. The membrane was washed again in TBST (3 × 10 min) and covered with enhanced chemiluminescent solution (Amersham Biosciences). After 1 min, excess enhanced chemiluminescent solution was poured off, and the membrane was sandwiched in a transparent sheet protector. Bands were then visualized using autoradiography film (Biomax MR Film; Kodak) in a safe-light darkroom. Tumor lysates were analyzed for levels of interleukin-8 (IL-8) using a human CXCL8/IL-8 ELISA (Quantikine; R&D Systems). All samples consisted of 160 μg total protein and were done in duplicate according to the manufacturer's protocol. The standard curve was generated using a four-variable logistic curve fit.

Statistics. Statistical analyses were done with Statistica software. One-way ANOVA was used to calculate P values. Differences were considered significant at $P \leq 0.05$.

Results

Irinophore C treatment inhibits growth and reduces the cell density of HT-29 tumors. All data presented were derived from tumors harvested from mice treated for 6 weeks. The inhibitory effect of Irinophore C on subcutaneous HT-29 tumors is shown in Fig. 1A. As outlined in Materials and Methods, mice were randomly assigned to 7 different groups when tumors were ~150 to 200 mm^3. Mice in the control group were treated with saline (□), and mice in the remaining groups were treated with Irinophore C for 3 weeks (●) or for 6 weeks with a 12-day break after week 3 (■). Treatment with Irinophore C inhibited tumor growth but did not cause tumor regression at this dose. When treatment was suspended, the tumors started to grow again within 5 to 8 days (●). If treatment was started again (■), further stabilization of the tumor was observed. Mice in the 6-week treatment group were sacrificed following imaging procedures to determine K_{trans}, and the tumors were collected for analysis as specified in Materials and Methods.

Tumor cell density was assessed by staining cell nuclei with Hoechst 33342. Image analysis of these sections indicated that the average intensity of Hoechst 33342 staining, summarized in Fig. 1B, was significantly lower for those tumors treated with 6 weeks of Irinophore C (■) (~35% lower; $P = 8.42 \times 10^{-5}$) compared with untreated tumors (□), reflecting a lower density of nuclei or cell density. H&E-stained tumor sections obtained from animals treated with saline or Irinophore C are shown in Fig. 1C. The tissue structure in untreated tumors is composed of densely packed cancer cells whose nuclei are stained dark purple and are permeated with river-like bands of stroma (pink). However, after treatment with Irinophore C, the density of the cancer cells is much lower and the tumor cells appear to be grouped in small islands amidst what appears to be fatty tissue, as determined by an experienced pathologist. Tumor cell nuclei from treated tumors are larger and lack prominent nucleoli, which are easily detected in tumors from saline-treated animals. Necrosis was not widespread or confluent and confined to single cells.

Irinophore C treatment is associated with a decrease in K_{trans}. Noninvasive magnetic resonance imaging was used to assess K_{trans}, the volume transfer constant of a solute between the blood vessels and extracellular tissue compartment of the tumor. The median viable values of K_{trans} for the tumors within the control and treated groups are graphed individually in Fig. 2A and show the relative spread of K_{trans} values between the control group (□) and the Irinophore C-treated group (■). The average values for K_{trans} in untreated tumors was ~1.5 times greater than in treated tumors (0.0375 and 0.025 mL/g/min for untreated and treated tumors, respectively; $P = 0.050$). The values for K_{trans} in untreated tumors were more variable compared with the treated group (SD = ±0.01 and ±0.001, respectively).

Irinophore C treatment is associated with increases in Hoechst dye perfusion and in the $CD31^+$ cells to tumor cell ratio. Hoechst 33342 dye was injected intravenously into the lateral tail vein

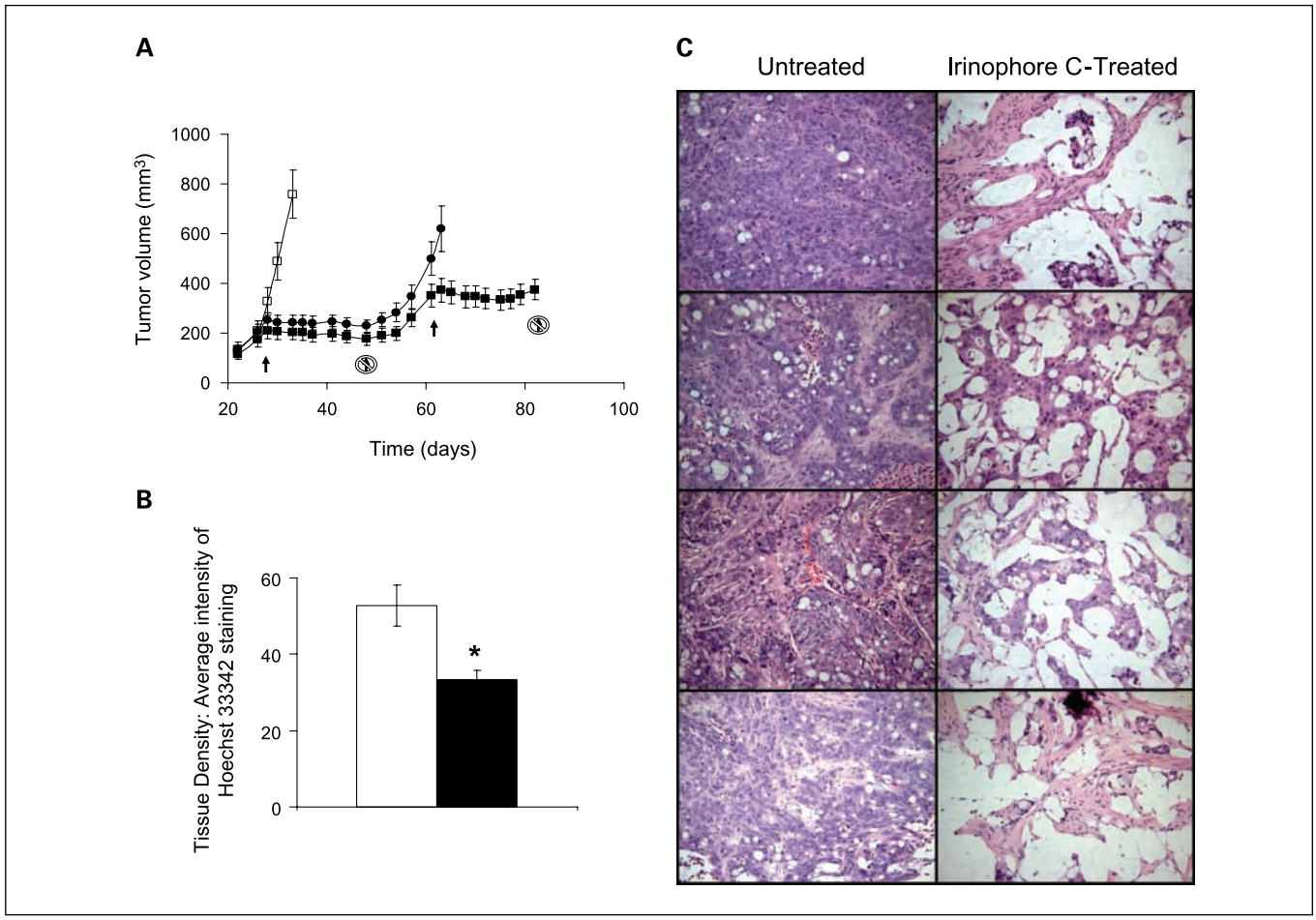

Fig. 1. *A* to *C,* Irinophore C treatment has a cytostatic effect on HT-29 tumors and reduces the cell density of the tumor. *A,* inhibitory effect of Irinophore C on HT-29 tumors grown subcutaneously in Rag2M mice. *Arrows,* start and end of treatment. Tumors in mice treated with saline reached predetermined endpoints within 2 wk and were harvested immediately (□). Tumor growth in mice treated with Irinophore C for 3 wk (●) or 6 wk with a 10- to 12-day break after week 3 (■) was inhibited, but the tumor was not eradicated. When treatment was suspended, the tumors started growing again (●); however, when treatment recommenced, growth was inhibited again (■). *B,* cell density of tumors treated with 6 wk of Irinophore C (■) was significantly reduced compared with untreated tumors (□). Cryosections of the tumors were flooded with Hoechst 33342 to stain cell nuclei as a measure of cell density. The average intensity of Hoechst 33342 staining shows that the cell density in treated tumors is reduced by ~35% ($P = 8.42 \times 10^{-5}$). *C,* images of H&E-stained tumor sections (magnification, ×20) from 4 sets of control and treated tumors show representative fields of view, clearly illustrating that the effect of Irinophore C is consistent in dramatically changing the tissue morphology and reducing the cell density.

of animals 20 min before tumor harvest to assess perfusion within the tumor. Significantly higher amounts of the fluorescent DNA-binding dye were found in tumors treated with Irinophore C. Figure 2B shows representative false-color composite images of cryosections from HT-29 tumors; Irinophore C-treated tumors contain greater quantities of dye labeling (blue) compared with controls. The proportion of pixels per unit area with staining intensity greater than threshold for Hoechst 33342 were quantified, and the data show that there is ~2.8-fold more Hoechst 33342 labeling in tumors from Irinophore C-treated animals (Fig. 2C; $P = 0.022$). The cryosections from HT-29 tumors shown in Fig. 2B were also stained for $CD31^+$ cells (green), and the results indicate that treatment with Irinophore C significantly decreased the number of $CD31^+$ pixels present in tumor sections. More specifically, tumor mapping analysis of entire sections showed that the overall percentage of $CD31^+$ pixels above threshold, as summarized in Fig. 2D, was significantly reduced ($P = 0.014$) in tumors from Irinophore C-treated animals (■) compared with untreated controls (□). Furthermore, when the percentage of $CD31^+$ pixels was normalized to the cell density, the results show a 1.8-fold increase in $CD31^+$ pixels relative to the number of tumor cells in the treated tumors compared with controls ($P = 0.00024$; Fig. 2E).

Irinophore C reduces tumor hypoxia. The level of tissue oxygenation in HT-29 tumors from control and Irinophore C-treated animals was examined with the hypoxic marker EF5. Because control, untreated tumors were substantially larger than treated tumors, the levels of hypoxia in the HT-29 model were first examined as a function of size. Untreated HT-29 tumors ranging from 200 to 600 mm^3 in size were exposed to EF5 as described in Materials and Methods. Subsequently, these tumors were disaggregated and analyzed with flow cytometry for the presence of viable hypoxic cells as reported previously (23). The results, plotted as a function of volume, are summarized in Fig. 3A and indicate that the percentage of viable hypoxia tumor cells is not correlated to size in HT-29 tumors ($R^2 = 0.0766$) within the range of volumes examined.

These results seemingly contradict previously published data where HT-29 tumors <1 mm in diameter were shown to be intensely hypoxic (and avascular) compared with tumors 1 to 4 mm in diameter (26); however, the size of tumors used in these studies were considerably larger (>0.5 cm^3). As shown in Fig. 3B, untreated tumors analyzed with flow cytometry were found on average to have a population of viable hypoxic levels of ~18% (consistent with the results shown in Fig. 3A), whereas treatment with Irinophore C for 6 weeks significantly reduced the population of viable hypoxic cells by 3-fold (~5% viable hypoxic cells; $P = 5.32 \times 10^{-9}$). Representative HT-29 sections for tumors from untreated and treated animals are shown in Fig. 3C and D, where a false-color image depicting cells stained positive for EF5 (red) is overlaid with an image for $CD31^+$ endothelial cells (green) against a hematoxylin background (gray). The images show that tumors from saline-treated animals have larger areas of hypoxic cells compared with tumors obtained from Irinophore C-treated animals.

Irinophore C treatment increases the accumulation of a second drug. Increased accumulation of Hoechst 33342 (Fig. 2C) and improvements in oxygenation levels (Fig. 3B-D) led us to investigate the effects of Irinophore C treatment on the delivery of 5-FU. The appearance of 5-FU in HT-29 tumors from animals treated with Irinophore C or saline was monitored with ^{19}F spectroscopy noninvasively over time in live animals. The doses used in this study were not meant to reflect therapeutically relevant doses but chosen to ensure a good signal-to-noise ratio for ^{19}F MRS. The amplitudes of the peak corresponding to the single fluorine atom in 5-FU, relative to an external standard (trifluoroacetic acid) and normalized to the tumor size, in individual control (□) and treated (■) mice are shown in Fig. 4A. The data suggest that the appearance of 5-FU is more variable in Irinophore C-treated tumors but that the tumors are exposed to up to 10 times more drug compared with untreated controls over the same period. The levels of bound ^{14}C-labeled 5-FU, added at tracer levels to the injected drug, in tumors from saline-treated (□) or Irinophore C-treated (■) animals were also measured using scintigraphy. The results show that ~1.5 times more 5-FU was present per gram of tumor tissue in tumors from Irinophore C-treated animals compared with

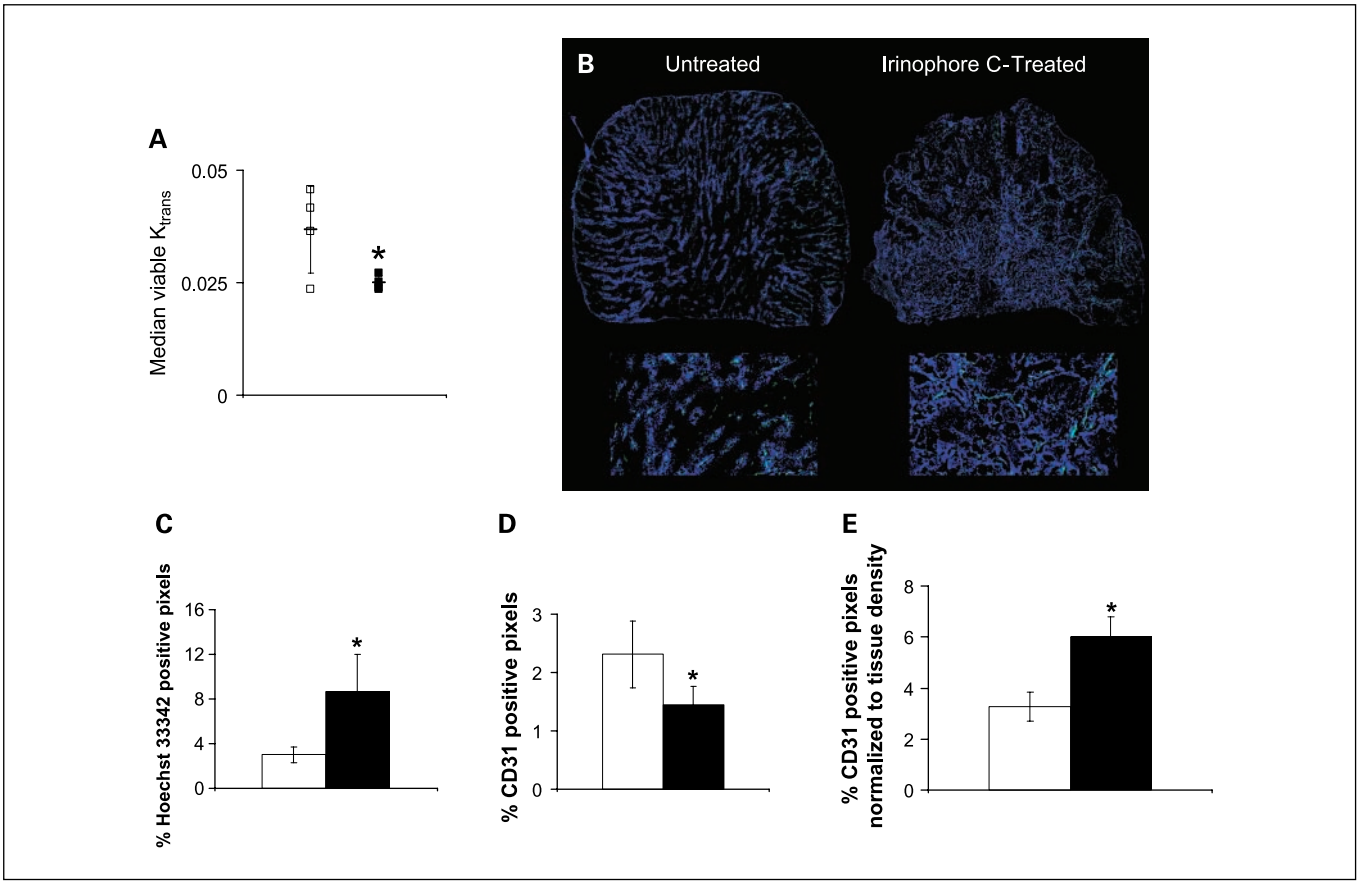

Fig. 2. *A* to *E,* vascular function in HT-29 tumors is improved with Irinophore C treatment. *A,* median viable values for K_{trans} in individual HT-29 tumors show the relative spread of K_{trans} values between the control group (□; 4 animals) and Irinophore C-treated group (■; 5 animals). The average value for K_{trans} (-) was significantly lower in the treated group ($P = 0.050$). The values for K_{trans} were more variable for the untreated group compared with the treated group of mice (SD = ±0.01 and ±0.001, respectively). *B,* significantly higher amounts of the fluorescent DNA-binding dye Hoechst 33342 injected intravenously are delivered to HT-29 tumors following treatment with Irinophore C relative to untreated controls. Representative images of sections from tumors harvested 20 min after intravenous injection of Hoechst 33342 (*blue*) show that more dye is present and that the overall amount of CD31 staining (*green*) is decreased in treated tumors. *C,* percentage of Hoechst 33342-positive pixels in sections from control (□) and treated tumors (■) was quantified, and the data show that ~2.8-fold more Hoechst 33342 is present in the Irinophore C-treated tumors ($P = 0.022$). *D,* tumor mapping analysis of sections stained specifically for endothelial cells indicates that the percentage of $CD31^+$ pixels per section in Irinophore C-treated tumors (■) is significantly reduced ($P = 0.014$) compared with untreated controls (□). Additional CD31 images can be seen in Figs. 3C and 4C. *E,* when the percentage of $CD31^+$ pixels is normalized to cell density (Hoechst 33342 flooding), a net 1.8-fold increase is seen ($P = 0.00024$) following treatment with Irinophore C.

controls (Fig. 4B; $P = 0.0002$). The scintigraphy data confirm, at a single time point, the ^{19}F spectroscopy data.

The accumulation of another commonly used anticancer drug, doxorubicin, was also evaluated in HT-29 tumor-bearing animals that were treated with saline or Irinophore C. Animals were injected with a single dose of doxorubicin (30 mg/kg) in animals treated with saline or with 6 weeks of Irinophore C. Size-matched tumors were subsequently harvested and the native fluorescence of bound doxorubicin present in the sections was visualized with fluorescence microscopy before subsequent staining and reimaging for endothelial cells (CD31) and nuclear density (Hoechst 33342 flooding). Representative false-color images of tumor sections from mice injected with doxorubicin are shown in Fig. 4C, where the native fluorescence of doxorubicin in tumors from mice treated with Irinophore C had a greater distribution compared with untreated control tumors. It should be noted that the cell density is not discernible in these images, and gaps in doxorubicin fluorescence within the tumors from Irinophore C-treated animals were associated with low tumor cell density (see Fig. 1B). Consequently, the visual assessment was corroborated by normalizing the average intensity of doxoru-

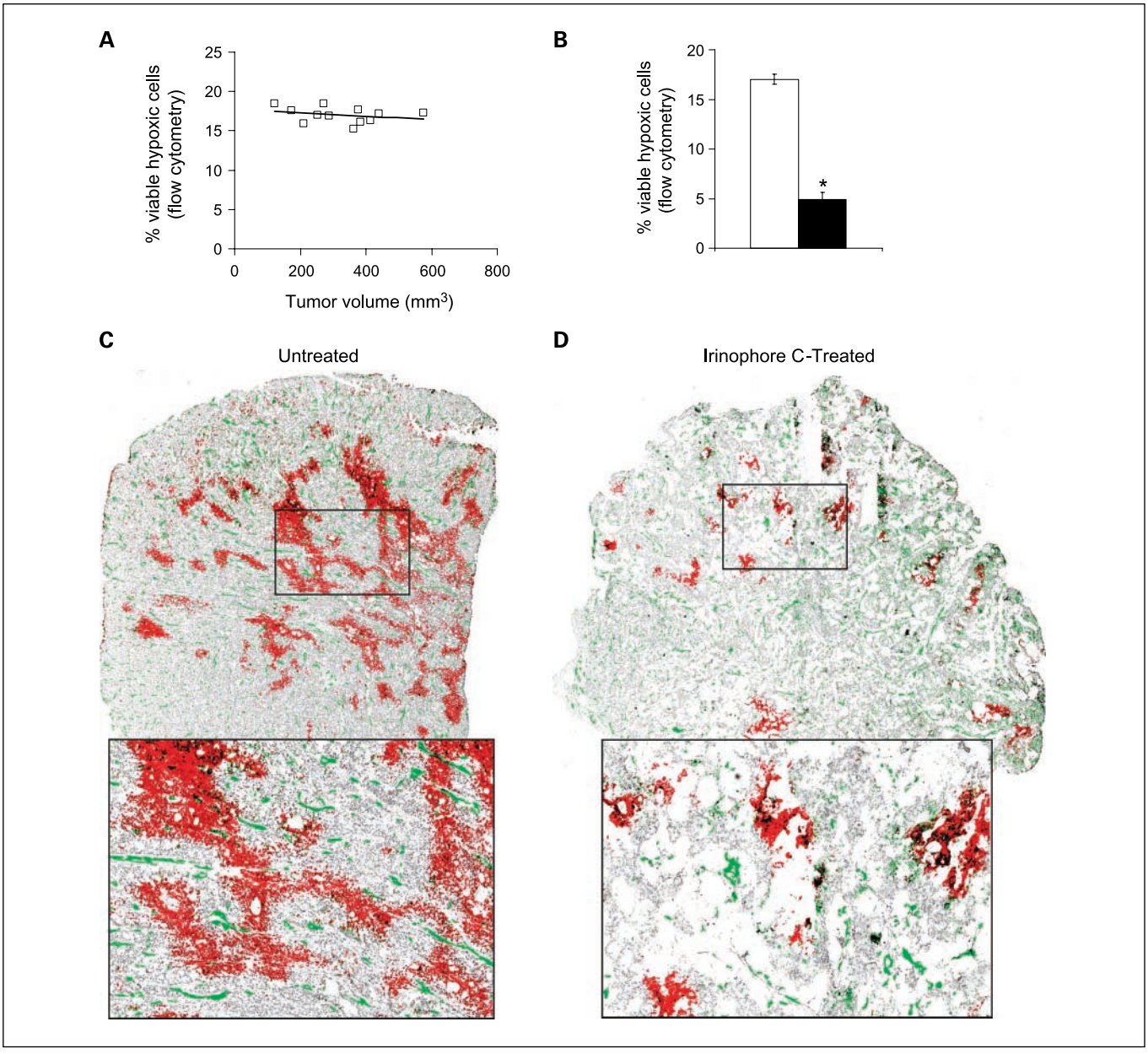

Fig. 3. *A* to *D,* Irinophore C treatment reduces levels of hypoxia in HT-29 tumors. *A,* percentage of viable hypoxic cells in untreated tumors ranging in size from 200 to 600 mm^3 was determined with EF5 staining and flow cytometry. No correlation was found between levels of hypoxia and the size of the tumor ($R^2 = 0.0766$). *B,* ~18% of viable cells in untreated tumors were found to be hypoxic; in contrast, Irinophore C-treated tumors were better oxygenated containing a significantly smaller population of viable hypoxic cells (~5%; $P = 5.32 \times 10^{-9}$). *C* and *D,* images of representative HT-29 sections with hypoxic and endothelial cells colored red and green, respectively, against a hematoxylin background show that untreated tumors have larger areas of hypoxic cells compared with the treated tumors. *Squares,* magnified images immediately below each section.

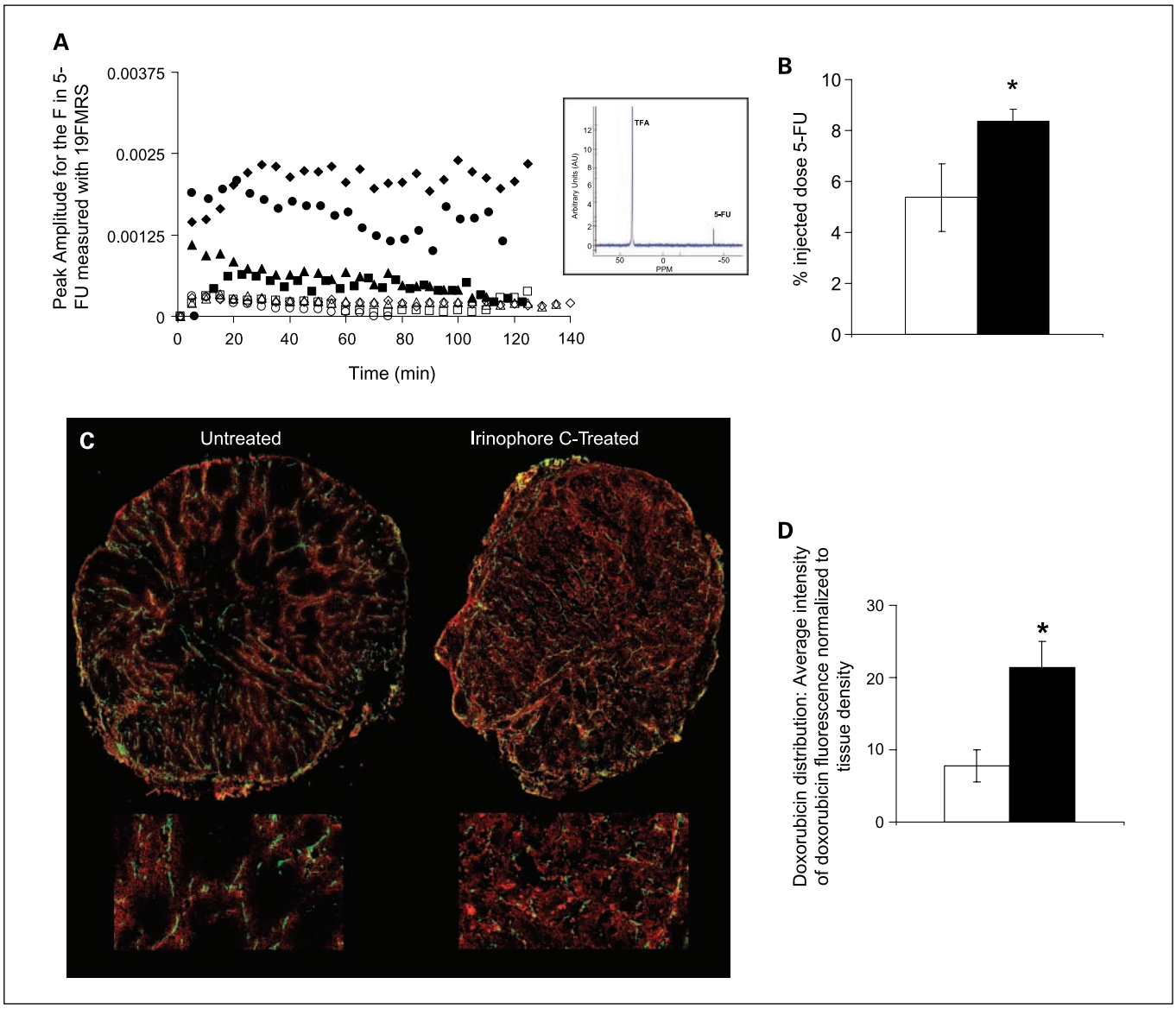

Fig. 4. *A* to *D,* treatment with Irinophore C increases the accumulation of a second drug in HT-29 tumors. *A,* ^{19}F spectroscopy was used to evaluate the delivery of 5-FU noninvasively in HT-29 tumors over 2 h in living animals. The relative amplitudes of the peak corresponding to the single fluorine atom in the 5-FU, normalized to an external standard (trifluoroacetic acid), in individual animals from untreated groups (□) and treated groups (■). *Inset,* representative spectrum for 5-FU measured *in vivo*. Data indicate that exposure of the tumor to 5-FU is more variable in Irinophore C-treated tumors but that higher concentrations of drug are present compared with untreated controls (up to 10-fold more drug in the same period). *B,* levels of [^{14}C]5-FU, added at tracer levels to the injected drug dose for ^{19}F MRS, bound to untreated tumors (□) and Irinophore C-treated tumors (■) were measured using scintigraphy. The percent injected dose of 5-FU present in the tumor tissue was ~1.5 times greater in Irinophore C-treated tumors compared with controls ($P = 0.0002$). *C,* similar results were obtained with the anticancer drug doxorubicin; control and Irinophore C-treated animals were injected with a single dose of doxorubicin, and the tumors were subsequently harvested and analyzed with fluorescence microscopy. The images of the tumor sections show that more doxorubicin is present in the Irinophore C-treated tumor tissue compared with untreated controls. *D,* average intensity of doxorubicin-positive pixels normalized to the cell density (Hoechst 33342 flooding) shows that Irinophore C-treated tumors (■) have significantly more doxorubicin present (~2.7-fold increase; $P = 0.2.43 \times 10^{-5}$) compared with control tumors (□).

bicin native fluorescence to the cell density as measured by the average intensity of flooded Hoechst 33342 staining. As summarized in Fig. 4D, in tumors from Irinophore C-treated animals (■), the amount of doxorubicin is ~2.7-fold greater than in control tumors (□; $P = 0.\ 2.43 \times 10^{-5}$).

Antiangiogenic and antivascular effects of Irinophore C. To better understand the observed effects of Irinophore C on tumor vasculature (see Fig. 2B and D), a survey of promoters and inhibitors of angiogenesis was completed. The results obtained from an ELISA screen of proangiogenic and antiangiogenic activators are summarized in Table 1. Two proangiogenic factors, VEGF and IL-8, were down-regulated and an inhibitor of angiogenesis, TIMP-1, was up-regulated in tumors from Irinophore C-treated animals compared with saline-treated controls. Other markers in the array were not detected by this assay, so no conclusions can be drawn regarding these activators and inhibitors. To confirm results obtained in the ELISA screen, Western blot analysis for VEGF

and TIMP-1 in tumor lysates from individual animals treated with saline or Irinophore C was completed. The results, shown in Fig. 5, corroborate the results of the initial screen for two forms of VEGF and for TIMP-1. An ELISA kit for human CXCL8/IL-8 (Quantikine; R&D Systems) was used to assess the levels of IL-8 in the treated and control tumors (154 and 265 pg/mL, respectively); a strong trend toward lower levels of IL-8 in treated tumors (~1.7-fold less) was observed, although the results did not achieve significance (P = 0.07).

Discussion

Lipid-based nanopharmaceuticals are reasonably well-established (27–29), and in the context of anticancer drugs, most investigators would suggest that the benefits of these drug carriers include prolonged systemic drug exposure, enhanced delivery of the associated drug to tumors, and/or protection of the associated drug from premature metabolism in the plasma. Drug carrier formulations of camptothecins have been aggressively pursued in part because the formulations improve the availability of the active lactone form of the drug (30). The liposomal formulation of irinotecan developed by our group (Irinophore C) maintains the drug in its active form within the liposome, extends its plasma half-life, and improves accumulation of drug in the tumor (16). Prolonged systemic exposure to the active form of irinotecan as well as its more active metabolite SN-38, along with other data suggesting that these drugs can have antivascular or antiangiogenic effects, prompted us to study the effects of Irinophore C on tumor morphology and vasculature. We recently reported that Irinophore C was significantly more active than irinotecan in 5 different xenograft models (17), so here we focus on one of those tumor models (HT-29) and completed a multimodality imaging analysis of tumor-associated vascular structure and function. The results of this study clearly show that Irinophore C treatment has a striking effect on the morphology and vasculature of the tumor. The changes in vascular structure and function have important implications for using this drug in a combination setting and, as discussed below, allow us to speculate on the potential use of this nanopharmaceutical to increase the penetration and accumulation of a second chemotherapeutic agent.

Table 1. Irinophore C treatment of HT-29 tumors inhibits angiogenesis

Activators			Inhibitors
ANG	IL-1α	FGF-α	IFN-γ
G-CSF	IL-1β	FGF-β	IL-12
HGF	IL6	TNF-α	IP-10
Leptin	*IL-8*	TGF-β	**TIMP-1**
VEGF	PIGF	*Negative controls*	TIMP-2
		Positive controls	

NOTE: Pooled tumor lysates from untreated and treated tumors were assayed with an ELISA-based screen of proangiogenic and antiangiogenic activators. The proangiogenic factors VEGF and IL8 were down-regulated in Irinophore C-treated tumors relative to untreated controls (italicized), whereas the inhibitor of angiogenesis TIMP-1 was up-regulated (bold). The remaining factors in the assay were not detected in either group of tumors.

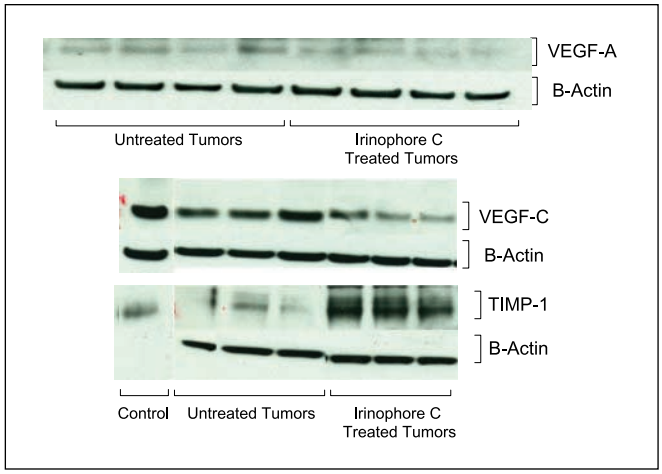

Fig. 5. Irinophore C treatment of HT-29 reduced expression levels of VEGF A and C but up-regulated expression levels of TIMP-1. Western blot analysis of the treated tumor lysates confirm that VEGF-A and VEGF-C were down-regulated (~2- and ~3.5-fold, respectively), whereas TIMP-1 was up-regulated (~4-fold) compared with untreated tumors.

It is notable that Irinophore C treatment stabilized the disease and did not cause tumor regression at these doses (Fig. 1A). This is similar to data that we have generated with a lipid-based formulation of vincristine, which when used to treat a human squamous cell carcinoma resulted in stable disease over an extended time course (31). Treatment effects that are associated with the appearance of stable disease are consistent with the observed effects obtained with metronomic chemotherapy (32, 33), where low doses of anticancer drugs are administered on a frequent or continuous schedule without extended breaks (33). The mechanistic basis of metronomic chemotherapy is believed to be primarily antiangiogenic, from either direct kill of endothelial cells in the growing tumor vasculature (34, 35) and/or destruction of bone marrow-derived endothelial progenitor cells (36, 37). The effects on tumor-associated endothelial cells is not necessarily surprising because many anticancer drugs, including irinotecan, have preferential activity against endothelial cells *in vitro* (38). In fact, the free drug was examined as an antiangiogenic agent in the late 1990s (39, 40) and was shown to inhibit neovascularization in a cornea model of angiogenesis (40). More recently, irinotecan was used to examine angiogenesis in a green fluorescent protein transgenic nude mouse model of human colon cancer (18). The use of irinotecan in a metronomic dosing regimen in a preclinical model of colorectal cancer (HT-29) was recently described (41); the authors indicate that metronomic dosing with irinotecan alone significantly inhibited tumor growth and also decreased microvessel density. The same group has now examined the pharmacokinetic and pharmacodynamic effects of metronomic irinotecan in metastatic colorectal patients, although the study did not include an examination of antivascular effects in the tumor tissue (42). Irinophore C, which behaves as a circulating drug depot that maintains low doses of active drug in the circulation for extended periods, may in fact be fundamentally akin to metronomic chemotherapy. We therefore speculate that the prolonged exposure to irinotecan and its active metabolite SN-38 (17) following intravenous use of Irinophore C may

elicit effects consistent with those achieved with metronomic dosing (42). Liposomal formulations of doxorubicin have also been shown to produce antivascular activity in models of glioma (43), which further corroborates our postulate that the liposomal formulation of Irinophore C indeed does have antiangiogenic effects.

Treatments with inhibitory effects on tumor vasculature have also been postulated to transiently and partially "normalize" the typically torturous, redundant, and inefficient vasculature found in tumors (44, 45). The concept of "vascular normalization" was originally conceived in 1972 (46) and more recently described in terms of a rebalancing of angiogenic processes gone awry in tumor growth (45). Whatever the precise mechanism behind this process, normalization of vasculature in window dorsal chamber tumor models treated with agents against VEGRF-2 improves blood flow and oxygen delivery to the cancer cells. These changes are associated with subsequent increases in drug penetration (47) and the sensitivity of the cells to radiation (48). Efficient delivery and distribution of anticancer agents is crucial in the treatment of solid tumors where every cancer cell, regardless of its local microenvironment, must be exposed to toxic levels of drug (49). Many small-molecule cancer therapeutics have shown evidence of poor tumor tissue penetration in both *in vitro* and *in vivo* model systems, including doxorubicin (50), gemcitabine (51), docetaxel, and paclitaxel (52). Thus, the concept of modifying the tumor vasculature, even temporarily, to improve radiotherapy by decreasing hypoxia, or increasing delivery of systemically administered chemotherapeutics, is highly compelling from the clinical perspective. The present studies indicate that Irinophore C treatment significantly decreases the number of endothelial cells and reduces K_{trans} while increasing the accumulation of the perfusion marker Hoechst 33342 in HT-29 tumors. The decrease in CD31 staining in treated tumors is consistent with an antiangiogenic effect (Fig. 2D). However, when CD31 staining is expressed relative to tumor cell density (see Fig. 2E), the ratio of endothelial cells to the number of cancer cells present in the section is actually $\sim$1.8-fold higher in treated tumors. Thus, relative to the size of the tumor, the overall vasculature is decreased; however, in terms of tumor cell density, the ratio of vasculature to tumor cells is increased presumably improving the coverage of the vascular network.

These data suggest that improved delivery of a second compound, as seen here with Hoechst 33342, 5-FU, and doxorubicin, would be expected based on the drug-induced changes in vascular structure and function. We also believe that decreases in K_{trans} values in tumors following treatment with Irinophore C are consistent with improved vascular function. If the vasculature is normalized in treated tumors, and vessels become less chaotic and leaky, then vessel permeability becomes the rate-limiting step for determining K_{trans}, and the values would be expected to drop, as was the case. Thus, the large variability in K_{trans} values associated with untreated tumors (see Fig. 2A) likely reflects the random nature of chaotic and leaky blood vessels in tumors (45). Leaky tumor vasculature allows the MR-visible contrast agent to enter the extracellular matrix easily, so blood flow is the rate-limiting step in the process and K_{trans} values in untreated tumors are more likely to approximate blood flow rates. The reduction of overall vasculature in the treated tumors may seem to be at odds with the levels of Hoechst 33342 delivered and one might expect that fewer blood vessels would be associated with reduced dye delivery to the tumor. However, the possibility that Irinophore C treatment may normalize tumor vasculature, rendering the vessels more functional and thus able to deliver more of the dye, is a reasonable interpretation of the results. Improved vascular function, as evidenced by the K_{trans} data, in combination with the dramatic changes to tissue morphology and density, may explain significantly enhanced accumulation of secondary agents in tumors from animals previously treated with Irinophore C.

The antiangiogenic effect of Irinophore C is corroborated by data showing that two promoters of angiogenesis, VEGF (53) and IL-8 (54), are down-regulated, whereas an inhibitor of angiogenesis, TIMP-1 (55), is activated in the treated tumors (see Table 1). VEGF-A is known to promote endothelial cell proliferation, sprouting, and tube formation; VEGF-C also contributes to angiogenesis by activating VEGF receptors (53). VEGF levels have also been correlated with vessel permeability (56); lower VEGF levels in treated tumors would be expected to decrease blood vessel permeability, further supporting the interpretation of the observed K_{trans} values. Evidence also exists for IL-8 being a stimulus for endothelial cell proliferation, tube formation, and endothelial cell survival (54). In contrast, TIMP-1 is a known inhibitor of matrix metalloproteinases, which are necessary for breaking down the extracellular matrix to permit endothelial cell invasion (55); an increase in expression levels of TIMP-1 would thus have an antiangiogenic effect by preventing this process. However, angiogenesis is a complex process and the precise molecular mechanisms behind the effects of Irinophore C on tumor vascular function is a focus of ongoing studies.

Because treatment with Irinophore C appeared to improve vascular function and accumulation of Hoechst 33342, the effect of treatment on hypoxia as well as the delivery and accumulation of a second drug in these tumors was examined. Tumor hypoxia in tumors from saline-treated and Irinophore C-treated tumors was evaluated with the EF5/ELK3-51 system, which is specific for viable hypoxic cells (20, 21). The data indicate that Irinophore C treatment significantly reduces the proportion of viable, hypoxic tumor cells and this may be equated with improved delivery of oxygen. A decrease in hypoxia would have important implications for scheduling radiation treatments in colon cancer as hypoxia adversely affects radiation treatment (57, 58). Enhanced accumulation and improved distribution of doxorubicin and 5-FU in HT-29 tumors from animals treated for 6 weeks with Irinophore C were significantly higher compared with untreated controls. Exposure of cancer cells to higher levels of either drug would presumably result in better cell kill, and it will be important to now study in preclinical models the influence of Irinophore C treatment in combination with second agents, either given simultaneously or sequentially. More specifically, the results reported here raise the intriguing possibility of using subsequent or concurrent therapies to take advantage of changes in the tumor microenvironment engendered by Irinophore C. Because 5-FU and irinotecan are used in combination (FOLFIRI) to treat colon cancer (3), restoring or improving vascular function in the tumor by replacing irinotecan with Irinophore C could be beneficial if it

improved the therapeutic efficacy of 5-FU by increasing the delivery and subsequent accumulation of the drug in the tumor. Likewise, the efficacy of ionizing radiation could be increased if tumor hypoxia is decreased by treatment with Irinophore C in an adjuvant setting. Our group thus believes that the potential for Irinophore C to change the tumor microenvironment and render cancer cells more vulnerable to sequential chemotherapy or radiotherapy is a novel observation with immediate implications for the treatment of advanced colon cancer. Although the results reported here are relevant to colon cancer, the basic principles should be applicable to all solid tumors because angiogenesis and the expansion of a vascular network is a requirement for tumor proliferation and metastasis.

Disclosure of Potential Conflicts of Interest

No potential conflicts of interest were disclosed.

Acknowledgments

We thank D. Masin and the animal group for expert help.

References

1. Hanna WC, Ponsky TA, Trachiotis GD, Knoll SM. Colon cancer metastatic to the lung and the thyroid gland. Arch Surg 2006;141:93–6.
2. Andre N, Schmiegel W. Chemoradiotherapy for colorectal cancer. Gut 2005;54:1194–202.
3. Gill S, Blackstock AW, Goldberg RM. Colorectal cancer. Mayo Clin Proc 2007;82:114–29.
4. Hoff PM, Ansari R, Batist G, et al. Comparison of oral capecitabine versus intravenous fluorouracil plus leucovorin as first-line treatment in 605 patients with metastatic colorectal cancer: results of a randomized phase III study. J Clin Oncol 2001;19:2282–92.
5. Van Cutsem E, Twelves C, Cassidy J, et al. Oral capecitabine compared with intravenous fluorouracil plus leucovorin in patients with metastatic colorectal cancer: results of a large phase III study. J Clin Oncol 2001;19:4097–106.
6. Zhang W, Gordon M, Lenz HJ. Novel approaches to treatment of advanced colorectal cancer with anti-EGFR monoclonal antibodies. Ann Med 2006;38:545–51.
7. Shih T, Lindley C. Bevacizumab: an angiogenesis inhibitor for the treatment of solid malignancies. Clin Ther 2006;28:1779–802.
8. Bir A, Tan W, Wilding GE, Lombardo J, Fakih MG. 5-Fluorouracil, leucovorin and oxaliplatin plus bevacizumab in the first-line treatment of metastatic colorectal cancer: a single-institute study. Oncology 2007;72:4–9.
9. Kang BW, Kim TW, Lee JL, et al. Bevacizumab plus 'FOLFIRI or FOLFOX as third-line or later treatment in patients with metastatic colorectal cancer after failure of 5-fluorouracil, irinotecan, and oxaliplatin: a retrospective analysis. Med Oncol 2008. Epub 2008 May 22.
10. Rodel C, Sauer R. Radiotherapy and concurrent radiochemotherapy for rectal cancer. Surg Oncol 2004;13:93–101.
11. Lidder PG, Hosie KB. Rectal cancer: the role of radiotherapy. Dig Surg 2005;22:41–8; discussion 9.
12. Hinnen P, Eskens FA. Vascular disrupting agents in clinical development. Br J Cancer 2007;96:1159–65.
13. Kanthou C, Tozer GM. Tumour targeting by microtubule-depolymerizing vascular disrupting agents. Expert Opin Ther Targets 2007;11:1443–57.
14. Jain RK. Lessons from multidisciplinary translational trials on anti-angiogenic therapy of cancer. Nat Rev Cancer 2008;8:309–16.
15. Duda DG, Jain RK, Willett CG. Antiangiogenics: the potential role of integrating this novel treatment modality with chemoradiation for solid cancers. J Clin Oncol 2007;25:4033–42.
16. Ramsay E, Alnajim J, Anantha M, et al. A novel liposomal irinotecan formulation with significant antitumour activity: use of the divalent cation ionophore A23187 and copper-containing liposomes to improve drug retention. Eur J Pharm Biopharm 2008;68:607–17.
17. Ramsay EC, Anantha M, Zastre J, et al. Irinophore C: a liposome formulation of irinotecan with substantially improved therapeutic efficacy against a panel of human xenograft tumors. Clin Cancer Res 2008;14:1208–17.
18. Ji Y, Hayashi K, Amoh Y, et al. The camptothecin derivative CPT-11 inhibits angiogenesis in a dual-color imageable orthotopic metastatic nude mouse model of human colon cancer. Anticancer Res 2007;27:713–8.
19. Ng SS, Sparreboom A, Shaked Y, et al. Influence of formulation vehicle on metronomic taxane chemotherapy: albumin-bound versus Cremophor EL-based paclitaxel. Clin Cancer Res 2006;12:4331–8.
20. Koch CJ, Evans SM, Lord EM. Oxygen dependence of cellular uptake of EF5 [2-(2-nitro-1H-imidazol-1-yl)-*N*-(2,2,3,3,3-pentafluoropropyl)acetamide]: analysis of drug adducts by fluorescent antibodies vs bound radioactivity. Br J Cancer 1995;72:869–74.
21. Lord EM, Harwell L, Koch CJ. Detection of hypoxic cells by monoclonal antibody recognizing 2-nitroimidazole adducts. Cancer Res 1993;53:5721–6.
22. Dragowska WH, Warburton C, Yapp DT, et al. HER-2/neu overexpression increases the viable hypoxic cell population within solid tumors without causing changes in tumor vascularization. Mol Cancer Res 2004;2:606–19.
23. Yapp DT, Woo J, Kartono A, et al. Non-invasive evaluation of tumour hypoxia in the Shionogi tumour model for prostate cancer with ^{18}F-EF5 and positron emission tomography. BJU Int 2007;99:1154–60.
24. Lyng H, Dahle GA, Kaalhus O, Skretting A, Rofstad EK. Measurement of perfusion rate in human melanoma xenografts by contrast-enhanced magnetic resonance imaging. Magn Reson Med 1998;40:89–98.
25. Tofts PS, Brix G, Buckley DL, et al. Estimating kinetic parameters from dynamic contrast-enhanced T(1)-weighted MRI of a diffusable tracer: standardized quantities and symbols. J Magn Reson Imaging 1999;10:223–32.
26. Li XF, Carlin S, Urano M, et al. Visualization of hypoxia in microscopic tumors by immunofluorescent microscopy. Cancer Res 2007;67:7646–53.
27. Bakker-Woudenberg IA, Lokerse AF, Roerdink FH. Antibacterial activity of liposome-entrapped ampicillin *in vitro* and *in vivo* in relation to the lipid composition. J Pharmacol Exp Ther 1989;251:321–7.
28. Madden TD, Janoff AS, Cullis PR. Incorporation of amphotericin B into large unilamellar vesicles composed of phosphatidylcholine and phosphatidylglycerol. Chem Phys Lipids 1990;52:189–98.
29. Nacucchio MC, Gatto Bellora MJ, Sordelli DO, D'Aquino M. Enhanced liposome-mediated antibacterial activity of piperacillin and gentamicin against Gram-negative bacilli *in vitro*. J Microencapsul 1988;5:303–9.
30. Burke TG, Bom D. Camptothecin design and delivery approaches for elevating anti-topoisomerase I activities *in vivo*. Ann N Y Acad Sci 2000;922:36–45.
31. Webb MS, Harasym TO, Masin D, Bally MB, Mayer LD. Sphingomyelin-cholesterol liposomes significantly enhance the pharmacokinetic and therapeutic properties of vincristine in murine and human tumour models. Br J Cancer 1995;72:896–904.
32. Glade Bender J, Cooney EM, Kandel JJ, Yamashiro DJ. Vascular remodeling and clinical resistance to anti-angiogenic cancer therapy. Drug Resist Updat 2004;7:289–300.
33. Kerbel RS, Kamen BA. The anti-angiogenic basis of metronomic chemotherapy. Nat Rev Cancer 2004;4:423–36.
34. Browder T, Butterfield CE, Kraling BM, et al. Antiangiogenic scheduling of chemotherapy improves efficacy against experimental drug-resistant cancer. Cancer Res 2000;60:1878–86.
35. Klement G, Baruchel S, Rak J, et al. Continuous low-dose therapy with vinblastine and VEGF receptor-2 antibody induces sustained tumor regression without overt toxicity. J Clin Invest 2000;105:R15–24.
36. Bertolini F, Paul S, Mancuso P, et al. Maximum tolerable dose and low-dose metronomic chemotherapy have opposite effects on the mobilization and viability of circulating endothelial progenitor cells. Cancer Res 2003;63:4342–6.
37. Shaked Y, Emmenegger U, Man S, et al. Optimal biologic dose of metronomic chemotherapy regimens is associated with maximum antiangiogenic activity. Blood 2005;106:3058–61.
38. Miller KD, Sweeney CJ, Sledge GW, Jr. Redefining the target: chemotherapeutics as antiangiogenics. J Clin Oncol 2001;19:1195–206.
39. Clements MK, Jones CB, Cumming M, Daoud SS. Antiangiogenic potential of camptothecin and topotecan. Cancer Chemother Pharmacol 1999;44:411–6.
40. O'Leary JJ, Shapiro RL, Ren CJ, et al. Antiangiogenic effects of camptothecin analogues 9-amino-20(*S*)-camptothecin, topotecan, and CPT-11 studied in the mouse cornea model. Clin Cancer Res 1999;5:181–7.
41. Bocci G, Falcone A, Fioravanti A, et al. Antiangiogenic and anticolorectal cancer effects of metronomic irinotecan chemotherapy alone and in combination with semaxinib. Br J Cancer 2008;98:1619–29.
42. Allegrini G, Falcone A, Fioravanti A, et al. A pharmacokinetic and pharmacodynamic study on metronomic irinotecan in metastatic colorectal cancer patients. Br J Cancer 2008;98:1312–9.
43. Zhou R, Mazurchuk R, Straubinger RM. Antivasculature effects of doxorubicin-containing liposomes in an intracranial rat brain tumor model. Cancer Res 2002;62:2561–6.
44. Jain RK. Normalizing tumor vasculature with anti-angiogenic therapy: a new paradigm for combination therapy. Nat Med 2001;7:987–9.
45. Jain RK. Normalization of tumor vasculature: an emerging concept in antiangiogenic therapy. Science 2005;307:58–62.
46. Le Serve AW, Hellmann K. Metastases and the normalization of tumour blood vessels by ICRF 159: a new type of drug action. Br Med J 1972;1:597–601.
47. Tong RT, Boucher Y, Kozin SV, et al. Vascular

normalization by vascular endothelial growth factor receptor 2 blockade induces a pressure gradient across the vasculature and improves drug penetration in tumors. Cancer Res 2004;64:3731–6.

48. Winkler F, Kozin SV, Tong RT, et al. Kinetics of vascular normalization by VEGFR2 blockade governs brain tumor response to radiation: role of oxygenation, angiopoietin-1, and matrix metalloproteinases. Cancer Cell 2004;6:553–63.

49. Minchinton AI, Tannock IF. Drug penetration in solid tumours. Nat Rev Cancer 2006;6:583–92.

50. Primeau AJ, Rendon A, Hedley D, Lilge L, Tannock IF. The distribution of the anticancer drug doxorubicin in relation to blood vessels in solid tumors. Clin Cancer Res 2005;11:8782–8.

51. Huxham LA, Kyle AH, Baker JH, Nykilchuk LK, Minchinton AI. Microregional effects of gemcitabine in HCT-116 xenografts. Cancer Res 2004;64:6537–41.

52. Kyle AH, Huxham LA, Yeoman DM, Minchinton AI. Limited tissue penetration of taxanes: a mechanism for resistance in solid tumors. Clin Cancer Res 2007;13:2804–10.

53. Otrock ZK, Mahfouz RA, Makarem JA, Shamseddine AI. Understanding the biology of angiogenesis: review of the most important molecular mechanisms. Blood Cells Mol Dis 2007;39:212–20.

54. Brat DJ, Bellail AC, Van Meir EG. The role of interleukin-8 and its receptors in gliomagenesis and tumoral angiogenesis. Neuro-Oncol 2005;7:122–33.

55. Chirco R, Liu XW, Jung KK, Kim HR. Novel functions of TIMPs in cell signaling. Cancer Metastasis Rev 2006;25:99–113.

56. Inai T, Mancuso M, Hashizume H, et al. Inhibition of vascular endothelial growth factor (VEGF) signaling in cancer causes loss of endothelial fenestrations, regression of tumor vessels, and appearance of basement membrane ghosts. Am J Pathol 2004;165:35–52.

57. Brown JM. The hypoxic cell: a target for selective cancer therapy. Eighteenth Bruce F. Cain Memorial Award lecture. Cancer Res 1999;59:5863–70.

58. Brown JM, Giaccia AJ. The unique physiology of solid tumors: opportunities (and problems) for cancer therapy. Cancer Res 1998;58:1408–16.